The Stability and Decomposition of Gaseous $[Mn(CO)_5]_2(\mu\text{-}SiH_2)$

G. T. Stauf, D. La Graffe, and P. A. Dowben

Laboratory for Solid State Science and Technology, Syracuse University, Syracuse, New York 13244-1130

K. Emrich, S. Barfuss, and W. Hirschwald

Institut für Physikalische Chemie, Freie Universität Berlin, Takustraße 3, 1000 Berlin 33, Federal Republic of Germany

N. M. Boag

Department of Chemistry and Applied Chemistry, Salford University, Salford, England, M5-4WT

Z. Naturforsch. **43a**, 758–764 (1988); received May 18, 1988

The ionic decomposition of gaseous bridge-bonded dimanganese silyl carbonyl $[Mn(CO)_5]_2(\mu\text{-}SiH_2)$ has been investigated via photon and electron induced ionization mass spectroscopy, as well as gas-phase photoabsorption measurements. The thermodynamic cycle incorporating ionic fragments has been constructed from these results. The thermodynamic cycle illuminates the decomposition process of this organometallic compound. This has potential application in the production of silicide Mn_2Si coatings by both pyrolysis and by patterned photolysis using an UV laser.

I. Introduction

Chemical vapor deposition (CVD) from organometallic compounds is a common way of creating metal and metal silicide coatings [1]. Deposition may be induced by pyrolysis, plasma processes, or by photolysis. Silicides, metal/silicon compounds in various phases and combinations, have found favor of late in the semiconductor industry when low-resistance interconnects capable of withstanding high temperatures are needed. While some commonly used organometallic source compounds such as alkyls, chlorides, and hydrides have been heavily investigated, little research has been done on more unusual sources. A molecule such as $[Mn(CO)_5]_2(\mu\text{-}SiH_2)$, which contains both the Mn and Si in a 2:1 stoichiometric ratio, if properly induced, decomposes to create a novel silicide in one step, thus avoiding the 2 or 3 gas flow-metering system now used for multicomponent coatings.

In order to control the decomposition of such a molecule, an understanding of the energetics of decomposition and bond breaking is certainly necessary. With few exceptions [2, 3] these are poorly understood. With the aim of understanding decomposition energetics we have therefore undertaken an electron impact mass spectroscopy, photoionization mass spectroscopy, and gas-phase photoabsorption investigation of $[Mn(CO)_5]_2(\mu\text{-}SiH_2)$.

In a plasma, positive ions are created from the ambient gas as a result of the impact of electrons into neutral gas molecules [4]. Similar processes, resulting in the creation of positive ions, occur in the ion source of a mass spectrometer, although the reactions of ions in a mass spectrometer do not always parallel those reactions found in commercial plasmas or electron and ion assisted deposition processes (which have much higher pressures and a wider range of impact energies). Incident electrons will, if sufficiently energetic, create positive ions, which may then be mass selected and detected. By characterizing the ionic decomposition products and associated energetics with a mass spectrometer, some processes that take place in a plasma can be investigated, and an ionic-decomposition side of the thermodynamic cycle built up [5–7].

II. Experimental

The $[Mn(CO)_5]_2(\mu\text{-}SiH_2)$ complex was prepared as described previously [8, 9].

The electron impact mass spectroscopy experiments were undertaken using a molecular beam of sample vapor generated in an alumina Knudsen cell.

Reprint requests to P. A. Dowben, Department of Physics, Syracuse University, 201 Physics Building, Syracuse, New York 13244-1130, USA.

0932-0784 88 0800-0758 $ 01.30/0. – Please order a reprint rather than making your own copy.

This beam was directed into the ionization region of the electron impact ion source of a Varian MAT single-sector magnetic field mass spectrometer. Ionization efficiency curves (IEC's), i.e. plots of ion intensity versus electron impact energy, were recorded under isothermal vaporization conditions in steps of 0.025 eV between 1 and 26 eV incident electron energy. Calibration, data reduction, evaluation procedure, and analysis of the fine structure of the IEC's were undertaken using procedures outlined elsewhere [10, 11].

The alumina Knudsen cell, used as a source for gaseous parent species, was encased in a tantalum mantle. The sample gas was generated from the Knudsen cell which contained equilibrium gas phase above the pure solid organometallic at temperatures between 300 and 350 K. A constant temperature in the Knudsen cell was used for each experiment. Experiments were repeated at several different temperatures and different corresponding effusion rates to confirm that results remained independent of pressure.

The fragmentation of $[Mn(CO)_5]_2(\mu\text{-}SiH_2)$ was also studied inside a high-temperature photoionization system using synchrotron radiation in the photon energy region 6–24 eV. The synchrotron radiation source was the electron storage ring BESSY (Berliner Elektronenspeicherring Gesellschaft für Synchrotronstrahlung mbH) in Berlin, BRD. The light was dispersed by a Wadsworth monochromator with a 1200 lines/mm MgF_2 coated Al parabolic grating and reflecting mirror. The ions were detected using a Balzers QMG 511 quadrupole mass spectrometer.

Photoabsorption data on the gaseous species were collected at the Tantalus Storage Ring at the University of Wisconsin Synchrotron Radiation Facility. A Normal Incidence Monochromator (NIM) was used to disperse light in the energy range 2–11 eV, while light intensity was monitored with a sodium salicylate coated window and photomultiplier. Sample vapor in equilibrium over the solid at 300 to 350 °K was admitted to the 1.5 m absorption tube, while photomultiplier counts were recorded as a function of monochrometer wavelength.

III. Results

The following major parent and fragment ions were identified with mass spectroscopy: $(Mn_2SiH_2)(CO)_{10}^+$, $(Mn_2SiH_2)(CO)_9^+$, $(Mn_2SiH_2)(CO)_8^+$, $(Mn_2Si)(CO)_8^+$, $(Mn_2SiH_2)(CO)_7^+$, $(Mn_2SiH_2)(CO)_6^+$, $(Mn_2SiH_2)(CO)_5^+$, $(Mn_2SiH_2)(CO)_4^+$, $(Mn_2SiH_2)(CO)_3^+$, $(Mn_2SiH)(CO)_3^+$, $(Mn_2SiH_2)(CO)_1^+$, and $Mn_2SiH_2^+$. Signals seen for $(Mn_2SiH_2)(CO)_7^+$ and $(Mn_2SiH_2)(CO)_6^+$ in the electron impact studies were too small to obtain useful appearance potentials (AP's), so AP energies for these fragments were only derived from the photoionization experiments. The ions with the same number of carbonyls, but which differ in the number of hydrogens on the Si, have been grouped together. We did not find fragments differing only by one or two hydrogens to have very different appearance potentials. Even at the highest energy setting available on the mass spectrometer, 70 eV, no additional fragments were seen, although more hydrogen loss was observed. None of the H_2 loss ions appeared in greater than 1% abundance at 70 eV, and total combined Mn_2Si fragment abundance at this energy, with or without H_2 present, was 27%. The ionization potentials (IP's) and appearance potentials we found are summarized in Table 1. A comparison of electron impact ionization and photoionization results is included in the table. Good agreement between the two techniques can be seen, with the largest difference, 0.4 eV, present only in the case of $(Mn_2SiH_2)(CO)_3^+$.

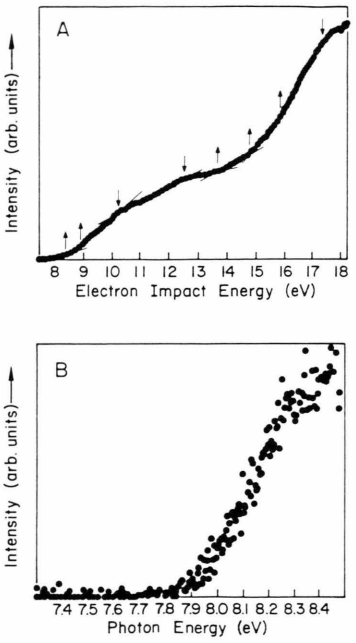

Fig. 1. (a) Ionization efficiency curve (IEC) from electron impact ionization for $[Mn(CO)_5]_2(\mu\text{-}SiH_2)$. Straight lines are drawn through appropriate segments of the plot, with slope changes indicated at arrows. (b) IEC from photoionization for $[Mn(CO)_5]_2(\mu\text{-}SiH_2)$.

Table 1. The ionization and appearance potentials based on the ionization efficiency curves of $[Mn(CO)_5]_2(\mu\text{-}SiH_2)$. Arrows designate relative increases (↑) and decreases (↓) of slope in the parent IEC's. Initial AP's are given both for electron and photoionization data, which are then averaged below, while higher AP's are from electron impact data only. Values are given in eV and rounded to tenths, as estimated error is ± 0.1 eV.

Species	AP (eV)	Relative increase (↑) or decrease (↓) of slope in parent IEC	*m/e* ratio
$[Mn(CO)_5]_2(SiH_2)^+$ (parent ion)	7.9 (electron)		420
	7.9 (photo)		
	7.9 (avg.)	↑	
	8.5	↑	
	8.7	↑	
	9.0	↑	
	10.4	↓	
	12.7	↓	
	13.8	↓	
	14.8	↑	
	15.9	↑	
	17.4	↑	
$Mn_2SiH_2(CO)_9^+$	8.4 (electron)		392
	8.4 (photo)		
	8.4 (avg.)	↑	
	9.1	↑	
	9.3	↑	
	9.8	↑	
	11.5	↑	
	12.7	↓	
	14.6	↑	
	16.5	↓	
	17.2	↓	
$Mn_2SiH_2(CO)_8^+$	9.4 (electron)		364
	9.4 (photo)		
	9.4 (avg.)	↑	
	10.2	↑	
	10.7	↑	
	11.6	↓	
	12.4	↓	
$Mn_2SiH_2(CO)_7^+$	10.7 (photo)		336
$Mn_2SiH_2(CO)_6^+$	11.0 (photo)		308
$Mn_2SiH_2(CO)_5^+$	12.6 (electron)		280
	12.6 (photo)		
	12.6 (avg.)	↑	
	13.6	↑	
	14.1	↑	
	15.9	↓	
	17.3	↓	

Species	AP (eV)	Relative increase (↑) or decrease (↓) of slope in parent IEC	*m/e* ratio
$Mn_2SiH_2(CO)_4^+$	13.6 (electron)		252
	13.6 (photo)		
	13.6 (avg.)	↑	
	14.4	↑	
	15.1	↑	
	15.6	↑	
	16.5	↑	
	17.3	↓	
	18.5	↓	
	21.3	↓	
$Mn_2SiH_2(CO)_3^+$	14.9 (electron)		224
	14.5 (photo)		
	14.7 (avg.)	↑	
	15.7	↑	
	16.1	↑	
	16.7	↑	
	19.6	↓	
$Mn_2SiH_2(CO)_2^+$	16.4 (electron)		196
	17.3	↑	
	17.8	↑	
	18.8	↑	
	20.0	↓	
	22.1	↓	
$Mn_2SiH_2(CO)_1^+$	17.1 (electron)		168
	17.0 (photo)		
	17.1 (avg.)	↑	
	18.0	↑	
	18.5	↑	
	19.0	↑	
	19.8	↑	
	22.6	↓	
$Mn_2SiH_2^+$	18.9 (electron)		140
	18.9 (photo)		
	18.9 (avg.)	↑	
	19.8	↑	
	20.4	↑	
	21.0	↑	
	21.6	↑	
	23.2	↑	
	25.2	↓	

Both ionization and appearance potentials for the parent and fragments were obtained from the ionization efficiency curves (IEC's). The IEC is, effectively, the molecular or fragment ion intensity plotted against the electron (or photon) impact energy employed to ionize the gaseous species, as shown in Figure 1. With increasing impact energy, a greater number of molecular orbital excitations become accessible, causing increases in the parent IEC intensity vs. energy slope. In addition, of course, these higher impact energies cause breakage of bonds within the molecule, and downward slope changes in the IEC. Thus, from the IEC, higher AP's may be estimated.

It should be noted that while photon impact provides very accurate IP's of the parent and first AP's of the fragment ions due to its high degree of monochromacity, it is not as useful for obtaining higher appearance potentials (slope changes) from IEC plots. This can be seen in Fig. 1, in IEC's derived from electron impact and photon impact of $(Mn_2SiH_2)(CO)_{10}$. The considerably better signal to noise ratio of the electron technique versus the photon technique is apparent.

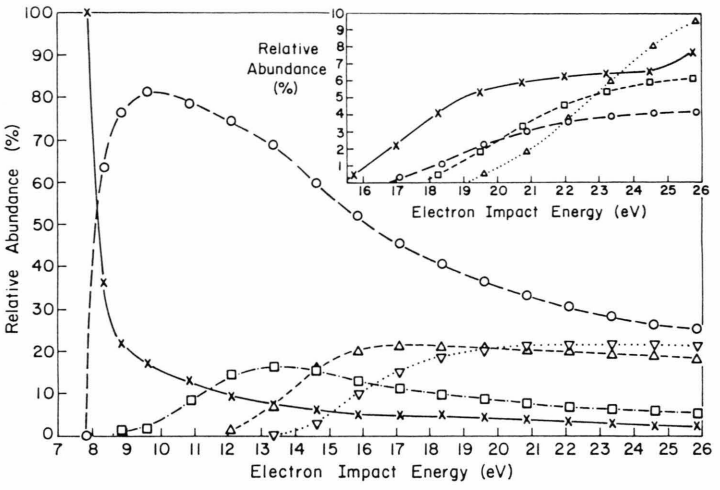

Fig. 2. The breakdown diagrams for $[Mn(CO)_5]_2(\mu\text{-}SiH_2)$ derived from electron impact IEC's. Relative intensities are plotted as functions of electron impact energy, with an intensity of 100% implying that this is the only observed fragment. Main plot: × ——— parent $(Mn_2SiH_2)(CO)_{10}^+$ ion, ○ — — $(Mn_2SiH_2)(CO)_9^+$ ion, □ – – – – $(Mn_2SiH_2)(CO)_8^+$ ion, △ – – – – $(Mn_2Si5_2)(CO)_5^+$ ion, ▽ ····· $(Mn_2SiH_2)(CO)_4^+$ ion. Corner inset plot: × ——— $(Mn_2SiH_2)(CO)_3^+$ ion, ○ —— $(Mn_2SiH_2)(CO)_2^+$ ion, □ – – – – $(Mn_2SiH_2)(CO)^+$, ion, △ ····· $Mn_2SiH_2^+$ ion.

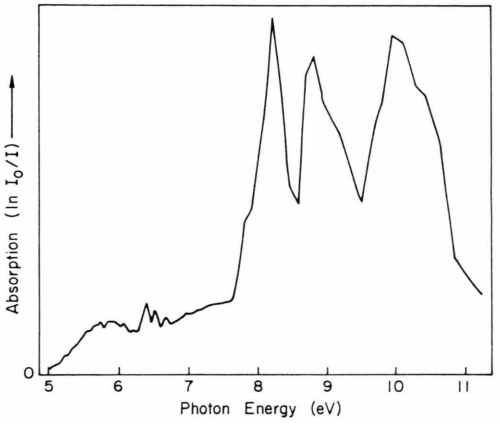

Fig. 3. Photoabsorption spectra for $[Mn(CO)_5]_2(\mu\text{-}SiH_2)$. Peaks represent increased absorption. Light in the vacuum ultraviolet range (2-11 eV) from the Tantalus Synchrotron in Wisconsin was passed through a KCl window and monochromated by a Normal Incidence Monochromator (NIM).

Table 2. Photoabsorption bands seen in Fig. 3, showing probable causes for absorption peaks (based on IP and AP data in Table 1).

Photoabsorption Bands	
Photon Energy	Assignment
5.8 eV	electronic excitation
6.5 eV	electronic excitation
7.9 eV	ionization potential
8.1 eV	photoionization
8.9 eV	photoionization and dissociation
10.1 eV	photoionization and dissociation

Higher AP's from IEC slope changes (seen in Table 1) are obtained from electron impact mass spectroscopy alone. The disadvantage of electron impact ionization, on the other hand, is that it lacks (compared to photoionization) high monochromacity, causing an exponential tail in electron impact derived IEC's. This exponential (rather than the desired linear) rise at the onset of ionization can be difficult to factor out during data analysis. Fortunately, a combination of the two ionization techniques acts to eliminate the uncertainties associated with either one alone.

The relative intensities of the parent and fragment ions are seen plotted in Fig. 2. They are based on electron impact data, because the magnetic sector mass spectrometer used for the electron impact studies was capable of better mass resolution than the quadrupole mass spectrometer used for photoionization, and was able to easily distinguish a 2 atomic mass unit separation.

The photoabsorption curve for this compound can be seen in Figure 3. Peaks indicate energy regions where strong absorption is taking place. These absorption bands are listed in Table 2.

VI. Discussion

The ionization potential and appearance potentials of the parent and fragment ions, listed in Table 1, are seen to be internally consistent. Not only do the photon and electron impact measurements agree, but the higher appearance potentials of the parent IEC can be related to the AP's of the fragment ions, as is seen in Table 3.

Table 3. Correlations between the fragment appearance potentials and slope changes (breaks) in the parent ion IEC are shown.

Ionic Fragmentation Correlations for the Parent $[Mn(CO)_5]_2(SiH_2)$		
Breaks in the parent IEC [eV]	Fragment AP [eV]	Fragment
8.5 (↑)	8.4	$Mn_2SiH_2(CO)_9^+$
10.4 (↓)	10.8	$Mn_2SiH_2(CO)_7^+$
12.7 (↓)	12.6	$Mn_2SiH_2(CO)_5^+$
13.8 (↑)	13.6	$Mn_2SiH_2(CO)_4^+$
14.8 (↑)	14.7	$Mn_2SiH_2(CO)_3^+$
15.9 (↑)	16.4	$Mn_2SiH_2(CO)_2^+$
17.4 (↓)	17.1	$Mn_2SiH_2(CO)^+$

From the relative abundances of the parent ion and different fragment ions (shown in Fig. 2) the $(Mn_2SiH_2)(CO)_{10}^+$, parent ion is seen to readily dissociate at energies greater than the appearance potential at about 8 eV. The first (and at low energies certainly the major) fragment formed is $(Mn_2SiH_2)(CO)_9^+$. An increase in the slope of the parent ion IEC is seen at 8.5 eV, close to the 8.4 eV at which the $(Mn_2SiH_2)(CO)_9^+$ ion appears. This indicates that the fragmentation mechanism involves a predissociation excitation, i.e. dissociation associated with an electronic excitation to an antibonding orbital. This partial filling of an antibonding orbital would weaken the carbonyl-metal bond leading to creation of the $(Mn_2SiH_2)(CO)_9^+$ ion. A downward slope change would indicate a direct bond breakage between the parent and the associated carbonyl fragments, since it decreases the amount of parent ion present while increasing the amount of the fragment ion seen.

Other fragments appear at higher energies, and for the most part remain relatively constant in percentage composition. An exception is the $Mn_2SiH_2^+$ fragment, which increases in percentage abundance with increasing electron impact energy range near 26 eV. This indicates that even in the high electron impact energy environment of a plasma, the core manganese-silicide cluster would survive the stripping away of carbonyl ligands, offering hope of deposition as a thin film with a well defined metal to silicon ratio of 2:1. The bonds between the two Mn's and the Si are obviously stronger than the bonds between each Mn and its CO ligands.

The photoabsorption spectra of $(Mn_2SiH_2)(CO)_{10}$ can be seen in Figure 3. The shoulder at 7.9 eV of the large peak centered around 8.2 eV clearly corresponds to the 7.9 eV ionization potential of the parent molecule. The large peaks at 8.2, 8.9 and 10.1 eV may also correspond to slope changes at 8.5, 8.7 and 10.4 eV in the electron impact IEC of $(Mn_2SiH_2)(CO)_{10}$ (described in Table 1).

We infer that the absorption band at 8.2 eV is an electron excitation which, together with some excess energy (possibly some 0.3 eV), may correspond to the multielectron ionization process associated with production of excited $(Mn_2SiH_2)(CO)_{10}^+$ with the partially filled antibonding orbital inferred from the electron impact mass spectroscopy results. The absorption bands at 8.9 and 10.1 eV must also be electronic excitations leading to photoionization, given the proximity (in energy) of these bands to IEC parent ion signal slope changes. These assignment are summarized in Table 2.

From the IP and AP information in Table 1, we were able to construct an ionic thermodynamic cycle for this compound. The ionic bond energies may be estimated as

$$D[(Mn_2SiH_2)(CO)_{10}^+ - CO] = AP[(Mn_2SiH_2)(CO)_9^+] - IP[(Mn_2SiH_2)(CO)_{10}] = 8.4 - 7.9 = 0.5\,eV,$$

$$D[(Mn_2SiH_2)(CO)_9^+ - CO] = AP[(Mn_2SiH_2)(CO)_8^+] - AP[(Mn_2SiH_2)(CO)_9^+] = 9.4 - 8.4 = 1.0\,eV,$$

$$D[(Mn_2SiH_2)(CO)_8^+ - CO] = AP[(Mn_2SiH_2)(CO)_7^+] - AP[(Mn_2SiH_2)(CO)_8^+] = 10.8 - 9.4 = 1.4\,eV.$$

Using only the photoionization appearance potential data from Table 1 for $(Mn_2SiH_2)(CO)_7^+$ and $(Mn_2SiH_2)(CO)_6^+$, since electron impact data for these fragments was not possible to assess, we see:

$$D[(Mn_2SiH_2)(CO)_7^+ - CO] = AP[(Mn_2SiH_2)(CO)_6^+] - AP[(Mn_2SiH_2)(CO)_7^+] = 11.0 - 10.8 = 0.2\,eV,$$

$$D[(Mn_2SiH_2)(CO)_6^+ - CO] = AP[(Mn_2SiH_2)(CO)_5^+] - AP[(Mn_2SiH_2)(CO)_6^+] = 12.6 - 11.0 = 1.6\,eV,$$

$$D[(Mn_2SiH_2)(CO)_5^+ - CO] = AP[(Mn_2SiH_2)(CO)_4^+] - AP[(Mn_2SiH_2)(CO)_5^+] = 13.6 - 12.6 = 1.0\,eV,$$

$$D[(Mn_2SiH_2)(CO)_4^+ - CO] = AP[(Mn_2SiH_2)(CO)_3^+] - AP[(Mn_2SiH_2)(CO)_4^+] = 14.7 - 13.6 = 1.1\,eV,$$

$$D[(Mn_2SiH_2)(CO)_3^+ - CO] = AP[(Mn_2SiH_2)(CO)_2^+] - AP[(Mn_2SiH_2)(CO)_3^+] = 16.4 - 14.7 = 1.7\,eV,$$

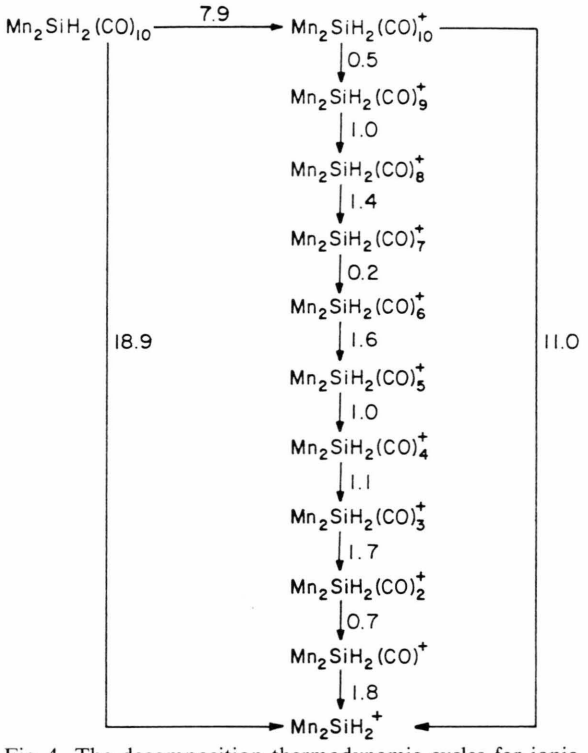

Fig. 4. The decomposition thermodynamic cycles for ionic fragmentation of $[Mn(CO)_5]_2(\mu\text{-}SiH_2)$, constructed from the AP/IP information in Table 1. The average AP and IP values listed (average between electron and photoionization data) were used. All numbers are in units of eV.

From electron impact IEC's from Table 1 for $(Mn_2SiH_2)(CO)_2^+$:

$$D[(Mn_2SiH_2)(CO)_2^+ - CO] = AP[(Mn_2SiH_2)(CO)^+] - AP[(Mn_2SiH_2)(CO)_2^+] = 17.1 - 16.4 = 0.7\,eV,$$

$$D[(Mn_2SiH_2)(CO)^+ - CO] = AP[Mn_2SiH_2^+] - AP[(Mn_2SiH_2)(CO)^+] = 18.9 - 17.1 = 1.8\,eV.$$

Thus we conclude that the total energy to go from the parent carbonyl to the Mn_2SiH_2 core is

$$D[(Mn_2SiH_2)(CO)_{10}^+ - 10(CO)] = AP[Mn_2SiH_2^+] - IP[(Mn_2SiH_2)(CO)_{10}] = 18.9 - 7.9 = 11.0\,eV.$$

From these calculations of bond strengths, we have constructed a thermodynamic cycle for the ionic decomposition of $(Mn_2SiH_2)(CO)_{10}$ which can be seen in Figure 4.

It will be noticed that larger energies are needed in the thermodynamic cycle to go from the $(CO)_8^+$ to $(CO)_7^+$ species, from $(CO)_6^+$ to $(CO)_5^+$, and $(CO)_4^+$ to $(CO)_3^+$ species (1.4, 1.6, and 1.1 eV, respectively). Therefore we can clearly see that symmetry considerations are important to molecular ion stability; i.e. some species with even numbers of carbonyls are more stable than those with odd numbers of carbonyl ligands. The mass spectra also clearly indicate that CO cleavage is always thermodynamically preferred over the Mn-Si bond breakage in highly energetic (impact energy $\geq$ IP) ionization processes, as is clear from the relative abundances in Figure 2. The activation energy for CO cleavage from $[Mn(CO)_5]_2(\mu\text{-}SiH_2)$ is similar to that observed for other metal carbonyl species [12–16], indicating that this molecule is fairly representative of the metal carbonyls despite having a three atom metal center (μ-$SiMn_2$).

We have formed coatings by pyrolysis at $\gtrsim 250\,^\circ C$ on Ni foil from this molecule [17]. Auger electron analysis (AES) and Rutherford back-scattering (RBS) have confirmed that the composition of the coatings was a stoichiometric one of Mn:Si = 2:1, as would be expected from our gas-phase work. Only small amounts of carbon and oxygen were found by RBS, aside from surface oxidation due to air exposure. Clearly the central metal-silicon cluster is depositing and losing its CO ligands under these conditions.

It is also apparent that for photolysis to take place, either an extremely energetic photon source must be used (11.0 eV = 103 nm), or an intensity sufficient for multi-photon reactions must be used, or some surface-activated process must be employed. Such a surface activated process has been observed in the deposition of Pd from allylcyclopentadienyl palladium on Si using 3.68 eV light [2]. The advantage of confining deposition to the surface rather than the gas phase, of course, is that substantially better line resolution would be obtainable when using a laser or mask.

V. Conclusions

We have constructed the thermodynamic decomposition cycle for gaseous dimanganese silyl carbonyl $[Mn(CO)_5]_2(\mu\text{-}SiH_2)$. Electron impact ionization, photoionization and photoabsorption were used to obtain ionization and appearance potentials with a high degree of confidence. This cycle and relative abundance information lead us to the conclusion that a high energy plasma should succeed in depositing stoichiometric compositions of Mn_2Si, as carbonyl ligands will be stripped off before the central Mn/Si cluster breaks apart. In addition, we believe that for photolysis to be practical, it would have to be a surface-activated process. This type of deposition has

been seen in photolysis previously [2], and would in any case be necessary for ultrafine line resolution.

Acknowledgements

This work was funded by the U.S. DOE through grant # DE-FG-02-87-ER-45319, the Deutsche Forschungsgemeinschaft/Sonderforschungsbericht 6 (DFG/SFB 6), the Freie Universität Berlin, and the Syracuse University Senate. We would also like to thank the staff of the Synchrotron Radiation Center (SRC) at Stoughton, Wisconsin and BESSY (Berlin, FRG). The SRC is supported by the National Science Foundation through grant DMR-86-01349.

[1] P. A. Dowben, J. T. Spencer, and G. T. Stauf, in preparation.
[2] G. T. Stauf, P. A. Dowben, K. Emrich, W. Hirschwald, and N. M. Boag, submitted.
[3] G. T. Stauf, D. C. Driscoll, P. A. Dowben, S. Barfuss, and M. Grade, Thin Solid Films **153,** 421 (1987).
[4] M. J. Rand, J. Vac. Sci. Technol. **16,** 420 (1979).
[5] D. C. Driscoll, J. A. Bishop, B. J. Sturm, P. A. Dowben, and C. G. Olsen, J. Vac. Sci. Tech. A **4,** 823 (1986).
[6] Y. J. Kime, D. C. Driscoll, and P. A. Dowben, J. Chem. Soc. Faraday Trans. II, **83,** 403 (1987).
[7] N. V. Zakurin, S. P. Gubin, and V. P. Bochin, J. Organomet. Chem. **23,** 535 (1970).
[8] B. J. Aylett and H. M. Colquhoun, J. Chem. Res. Synopses **6,** 148 (1977).
[9] K. M. Abraham and G. Urry, Inorg. Chem. **12**, 2850 (1973).
[10] M. Grade, J. Wienecke, W. Rosinger, and W. Hirschwald, Ber. Bunsenges. Phys. Chem. **87,** 355 (1983).
[11] W. Rosinger, M. Grade, and W. Hirschwald, Ber. Bunsenges. Phys. Chem. **87,** 536 (1983).
[12] C. M. Melliar Smith, A. C. Adams, R. H. Kaiser, and R. A. Kushner, J. Electrochem. Soc. Solid State Sci. Tech. **121,** 298 (1974).
[13] H. E. Carlton and J. G. Oxley, Amer. Inst. Chem. Eng. J. **13,** 86 (1967).
[14] H. E. Carlton and J. G. Oxley, Amer. Inst. Chem. Eng. J. **11,** 79 (1965).
[15] R. K. Chan and R. McIntosh, Can. J. Chem. **40,** 845 (1962).
[16] J. S. Foord and R. B. Jackman, Chem. Phys. Lett. **112,** 190 (1984).
[17] G. T. Stauf, P. A. Dowben, N. M. Boag, L. Morales de la Garza, and S. L. Dowben, Thin Solid Films **156,** 327 (1988).